Quantitative impact of structural inheritance on present-day deformation and seismicity concentration in intraplate deformation zones

Alizia Tarayoun, Stephane Mazzotti, Frédéric Gueydan

Quantitative impact of structural inheritance on present-day deformation and seismicity concentration in intraplate deformation zones

Alizia Tarayoun[a], Stephane Mazzotti[a], and Frédéric Gueydan[a]

[a] Géosciences Montpellier, Université de Montpellier, CNRS, Montpellier, France

Corresponding author: A. Tarayoun, alizia.tarayoun@hotmail.fr

Highlights

- Quantification of strain localization linked with structural inheritance.
- Impact of brittle and ductile lithospheric weakening on strain localization.
- Parametric study of strain localization in intraplate deformation zones.

Abstract

Structural inheritance (i.e. paleo-tectonic) areas, acting as weakened domains, appear to be a key element localizing the seismicity in intraplate deformation zones. However, the impact of structural inheritance on the observed present-day seismicity and strain rate concentration remains to be quantified. In this study, we quantify through 2D numerical modeling the localization and amplification factor of upper crustal strain rates induced by structural inheritance. Our 2D models are constrained by intraplate velocity boundary conditions and include rheology laws that accounts for inherited strain weakening in both the brittle and ductile layers of the lithosphere. The role of structural inheritance is investigated for different localization of the weakened domain in the lithosphere. For an average intraplate geotherm (Moho temperature ca. 500°C), brittle weakening (i.e. inherited faults) alone induces a limited amplification factor of upper crustal strain rates of ca. 4. Ductile weakening can increase the amplification factor to ca. 7 when localized in the lower crust, but has no effect when

localized in the lithospheric mantle. Overall, the amplification factors of upper crustal strain rates vary between 1 and 27 depending on the location of the weakened area in the lithosphere and on the different possible net driving forces, crustal strengths, amounts of weakening, and geotherms. These model amplification factors are in reasonable agreement with those derived from GPS and seismicity data over large spatial scale (several hundreds of kilometers) in North America.

Keywords

Intraplate deformation zones, Structural inheritance, Rheology weakening, Strain rate amplification factor, Strain concentration

1. Introduction

Present-day strain and seismicity in continental intraplate regions are not randomly distributed (Fig. 1a). It is commonly proposed that the localization of intraplate seismicity is related to the presence of structural inheritance zones (Coppersmith et al., 1987; Johnston, 1989; Adams and Basham, 1991), which act as weakened domains (Sykes, 1978). Depending on the metrics (number of events, moment budget, etc.), 55–95% of intraplate seismicity is localized in regions of structural inheritance (Johnston, 1989; Schulte and Mooney, 2005). In these studies, structural inheritance is defined as lithospheric-scale tectonic inherited structures (commonly Paleozoic and older). As a consequence, structural inheritance is associated with large domains (tens of kilometers) of significant lithospheric deformation (strain over 100%), mostly related to paleo-rifts or passive margins (Johnston, 1989).

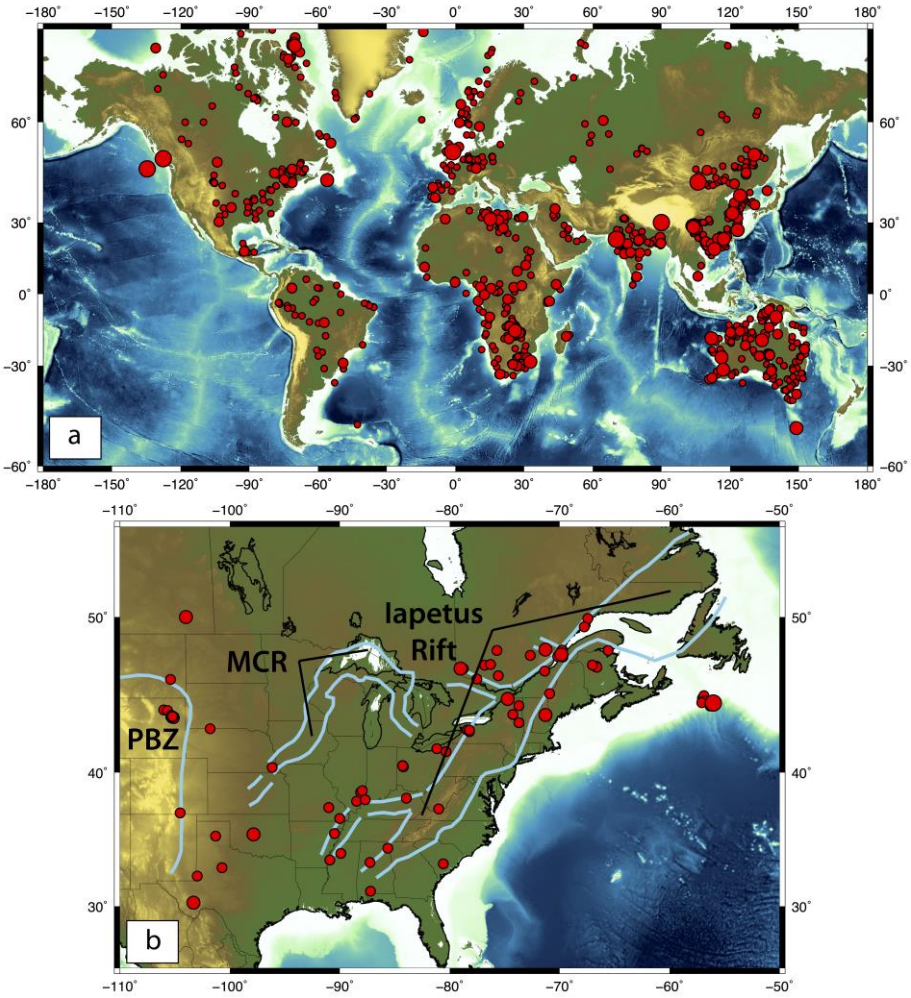

Figure 1. Intraplate seismicity. a/ Global intraplate earthquake catalog (USGS National Earthquake Information Center). Historical and instrumental earthquakes shown for magnitudes superior to 4.5 from AD. 495 to 2002. b/ Intraplate seismicity of Central and Eastern Canada and United States. Blue lines delimit main tectonic features: eastern edge of North America Plate Boundary Zone (PBZ), Mid-Continent Rift (MCR), Iapetus rifted margin and grabens.

Domains presenting structural inheritance are for instance the Iapetus rift in the St Lawrence Valley, eastern Canada and U.S.A (Kumarapeli, 1966), the Rhine graben in north-western Europe (Illies, 1972) or the Hercynian system associated with the South Armorican Shear Zone, western France (Jégouzo, 1980). The observed relation between the presence of

structural inheritance and the presence of seismicity is not always verified (Schulte and Mooney, 2005). For example, in the stable continental region of North America (Fig. 1b), seismicity appears to be mostly located along the paleo-rift Iapetus. Conversely, very little seismicity is associated with the Mid Continental Rift (MCR). One of the important consequences of this variability is the integration of structural inheritance in seismic hazard assessment that remains a current challenge (Stein and Mazzotti, 2007).

Although strain observation in intraplate regions is challenging compared to plate boundary system, seismic and GPS observations can constrain strain rates in term of order of magnitude. For instance, first-order estimations of seismic and GPS strain rates in central and eastern United Stated or eastern Canada are about 10^{-12}–10^{-8} yr^{-1} (Anderson, 1986; Mazzotti and Adams, 2005) and 10^{-10}–10^{-8} yr^{-1} (Mazzotti et al., 2005; Tarayoun et al., 2018).

Only few studies quantify the impact of structural inheritance on the observed strain and seismicity rates in intraplate domains. In eastern Canada, GPS observations show that structural inheritance amplifies strain rates by a factor of 2-11 (Tarayoun et al., 2018). The impact of a weak zone on surface deformation, which has been studied for various weakening sources, vary between factors of 3-4 (Wu and Mazzotti, 2007) to 100-1000 (Grollimund and Zoback, 2001; Mazzotti and Gueydan, 2017). A significant decrease of viscosity in the lower crust (Kenner and Segall, 2000) or in the lithospheric mantle (Grollimund and Zoback, 2001) can generate strain rate concentrations of 1-3 orders of magnitude in the New Madrid seismic zone, eastern United States. Wu and Mazzotti (2007) investigate the impact of a weak zone in a glacial isostatic adjustment model and show that surface strain rates increase by a factor up to 8 in eastern Canada. Mazzotti and Gueydan (2017) calculate strain rates associated with 1D lithospheric yield stress profiles integrating new rheology laws based on field observations (i.e. mylonite and proto-mylonite) that allow a link between structural inheritance and the reduction of viscosity in both the crust and mantle. They show that to explain observed GPS

and seismic strain rates, the crust and lithospheric mantle in intraplate deformation zones must be significantly weakened. The latter study assumes a lithosphere at near-failure equilibrium implying constant strain rates with depth. In low strain regions such as intraplate deformation zones, whole-lithosphere near-failure equilibrium may not be reached due to the existence of an elastic layer (or elastic core, cf. Kusznir, 1991) between brittle deformation in the upper part of the lithosphere and ductile deformation in the middle or lower parts. The presence of such elastic layers could result in significant effects on strain rate concentration in weak areas.

In this paper, we provide first quantitative estimations of the impact of structural inheritance on present-day surface deformation in intraplate deformation zones, i.e. seismically active intraplate regions. We do not attempt to provide quantification of structural inheritance impact in stable continental regions (i.e. cratons) where the active deformation is either not measurable or very poorly constrained. Our study is based on 2D numerical mechanical models. Our models are tuned to intraplate deformation zones conditions (boundary conditions and geotherm) and integrate inherited weakening through a rheology scaling based on field observations (Gueydan et al., 2014). In order for our model to be generic for all intraplate deformation zones, we assume a general weakened domain of several 10s km scale (cf. Gorczyk et al., 2012). In other words, we do not investigate the impact of a single fault or a single shear zone but rather, the structural inheritance domain represents the averaged effect of numerous faults and shear zones of any geometry. We focus our analysis on five scenarios testing different inheritance localization (Fig. 2): (1) a non-weakened lithosphere; (2) a weakened domain only in the brittle crust; (3) a weakened domain in the entire crust; (4) a weakened domain only in the lithospheric mantle; (5) a whole weakened lithosphere. The five scenarios are meant to represent all intraplate deformation zones, from a thick-skin thrust system for upper crust inheritance (for instance the Appalachians Province,

Eastern Canada; Thomas, 2006) to a rift structure for whole lithosphere inheritance (for instance the paleo Iapetus rift).

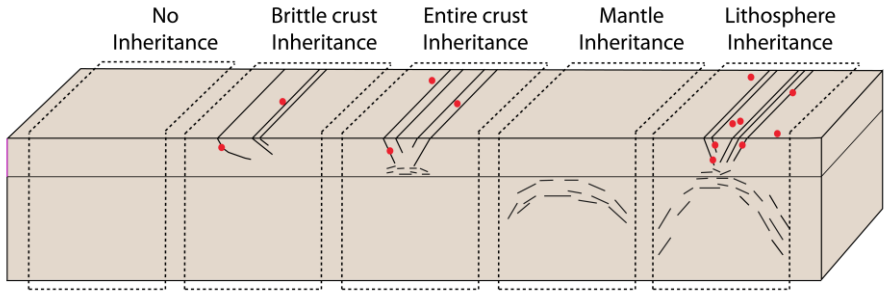

Figure 2. Conceptual scenarios of possible structural inheritance localization in the lithosphere and associated earthquakes (red dots).

We quantify the amplification factor of present-day upper crustal strain rates related to each scenarios using velocity boundary conditions coupled with an integrated lithospheric strength control, in order to take into account fully elasto-visco-plastic deformation. Compared to previous modeling studies, the main novelties of our study are, first, the use of 2D numerical models that allow taking into account variations of strain rates both laterally and with depth. This point allows robust results of the concentration of upper crustal deformation associated with lower-crust and upper-mantle weakened domains. Second, we quantify the role of inherited weakening within the conditions of a fixed net driving force. This point allows investigating the strength of the lithosphere and, thus, the associated upper crustal strain rates at different mechanical stages before reaching steady-state deformation.

2. Numerical model setup

2.1 Rheology

2.1.1 Reference rheologies (non-weakened lithosphere)

The mechanical behavior of the lithosphere is defined by brittle and ductile rheology laws, commonly presented as yield stress profiles, which correspond to the minimum between brittle and ductile differential stresses for given depths, temperature profiles and strain rates. Hereafter, we use analytic yield stress profiles to compare with differential stress profiles derived from the numerical models at various mechanical stages (cf. section 3). In analytic profiles, the brittle yield stress is equal to the Mohr-Coulomb stress (Byerlee, 1978):

$$\sigma_B = p * \sin(\phi_B) + C * \cos(\phi_B) \qquad (1)$$

where p is the lithostatic pressure (density of 2.7 g.m^{-3} and 3.3 g.m^{-3} for the crust and mantle, respectively), C the cohesion (10 MPa) and ϕ_B the internal friction angle (30°) as defined by Byerlee (1978). In the numerical model, the brittle stress is equal to the Drucker-Prager stress (Chéry et al., 2001), which is an approximation of the Mohr-Coulomb failure criterion (Owen and Hinton, 1980):

$$J_2 = \frac{-1}{3} J_1 + \frac{C}{\tan(\phi_D)} \qquad (2)$$

where J_1 and J_2 are the first and the second invariants of the stress tensor, respectively. To equalize the internal friction angle between Mohr-Coulomb and Drucker-Prager laws, we set ϕ_D at 15° (Chéry et al., 2001).

In both analytic and numerical models, the ductile yield stress σ_D is derived from the dislocation creep law (Weertman, 1978):

$$\sigma_D = \left(\frac{\dot{\varepsilon}}{A}\right)^{-n} * exp\left(\frac{Q}{nRT}\right) \qquad (3)$$

where $\dot{\varepsilon}$ is the strain rate (s^{-1}), T the temperature (K) and R the gas constant ($8.31\ J\ mol^{-1}\ K^{-1}$). As a first-order approximation of lithospheric mineral composition, quartz and olivine rheology parameters are used for crust and mantle, respectively ($A = 1.1x10^{5}$ and $3.9x10^{-10}\ Pa^{-n}s^{-1}$, $Q = 135$ and $530\ J.mol^{-1}$, and $n = 4$ and 3.5; Hirth and Kohlstedt, 2003; Luan and Paterson, 1992). A stronger rheology in the crust will also be considered (section 5.1).

2.1.2 Weakened rheologies

Several mechanisms inducing inherited strain weakening have been proposed. In the brittle crust, maturation of fault zones is achieved by nucleation of new minerals, such as mica or talc, decreasing the friction coefficient from ca. 0.6 to 0.1 (Holdsworth, 2004). In the ductile crust, intense weakening is related to the progressive development of layering (shear zone or foliation) enriched in mica (Wintsch et al., 1995; Gueydan et al., 2003). Shear heating is also proposed as a weakening process in the deep crust (Regenauer-Lieb and Yuen, 2003; Thielmann and Kaus, 2012). In the lithospheric mantle, two main processes could promote inherited strain weakening: grain size reduction during dynamic recrystallization of olivine (Hirth and Kohlstedt, 2003, Précigout and Gueydan, 2009) and preferred orientation of olivine leading to an inherited anisotropy (Tommasi et al., 2009).

Annealing (dynamic or static recrystallization) and reduction or suppression of the inherited weakening is possible if an event involving a significant increase of temperature (e.g., tectonic event or hotspot) occurs after the formation of the structural inheritance (Boneh et al., 2017). In an intraplate deformation zone where no major tectonic event has occurred since Paleozoic, and with generally low geotherms, we can assume that, in most cases, no annealing has taken place and thus the mechanisms of inheritance weakening are maintained through time.

In this study, we model inherited weakening using a generic expression that can represent any of the weakening processes listed above. Following Mazzotti and Gueydan (2017), we introduce an inherited strain-weakening rheology law that consists in integrating a finite weakening in the standard brittle and ductile rheology laws (section 2.1.1). The effect on differential stress of this finite weakening, based on field observations, is from the study of Gueydan et al. (2014):

$$\sigma = \sigma_0 * \left[1 + \alpha * \left(exp^{\frac{-\varepsilon}{\varepsilon_c}} - 1\right)\right] \qquad (4)$$

where σ_0 is either the initial brittle stress ($\sigma_B, J_2, Eqs. 1-2$) or ductile stress ($\sigma_D, Eq. 3$), α represents the maximum strain weakening factor (reduction of strength or effective viscosity for brittle and ductile behavior, respectively), ε the finite inherited strain of the considered domain and ε_c the characteristic strain over which the deforming rock fabric changes according to layering development (in the crust) or grain size reduction (in the mantle). The maximum strain weakening ($\alpha = 0.9$) and the characteristic strain ($\varepsilon_c = 0.5$) are based on numerical experiments of large deformation (Gueydan et al., 2014).

Thus, in our model, the amount of effective weakening is controlled by the finite strain parameter, ε, specific to a given region. As we defined structural inheritance as lithospheric-scale paleo-structures, we assume a large finite strain ($\varepsilon = 2$), equivalent to a stress scaling factor of 0.12. Lower finite strain will be tested (section 5.1). The weakening effect is restricted to small temperature ranges: from 0°C to 500°C and from 600°C to 800°C for the crust and mantle, respectively. Outside those ranges of temperature, the weakening disappears due to the mineral transformations leading to possible hardening in the crust (Gueydan et al., 2014) and to the lower impact of grain size reduction phenomenon in the mantle (Précigout and Gueydan, 2009).

2.1.3 Weakening impact on lithospheric yield stress profiles

In order to illustrate the effect of the weakening laws, we calculate analytic yield stress profiles for the five scenarios presented in Figure 2: non-weakening (NW), Upper Crust Weakening (UCW), Entire Crust Weakening (ECW), Mantle Weakening (MW) and whole Lithosphere Weakening (LW). Results are presented in Figure 3. Yield stress profiles are calculated for a finite inherited strain $\varepsilon = 2$ and with a constant strain rate with depth $\dot{\varepsilon} = 5.6$ x 10^{-17} s^{-1}, which corresponds to the bulk deformation expected in the numerical modeling. We use the Moho temperature, T_M, as a proxy for the geotherm. The surface temperature is set at 0°C, T_M at 500°C and the base of the lithosphere (150 km-depth) at 1300°C. The crustal thickness is 40 km, which is a reasonable average for continental intraplate regions (Mooney et al., 1998).

With non-weakening (Fig. 3a), the maximal yield stresses (at the brittle-ductile transitions) are 235 and 883 MPa for the crust and mantle, respectively. With an upper crust weakening, the maximal yield stress at the crustal brittle-ductile transition drops to 76 MPa (Fig. 3b). Ductile weakening in the lower crust has a low impact on strength reduction (Fig. 3c). The major weakening impact is in the lithospheric mantle between 40 and 80 km depth, where the maximal yield stress drops to 706 MPa (Fig. 3d). With a whole lithosphere weakening (Fig. 3e), the maximal yield stresses drop to 50 and 706 MPa for the crust and mantle, respectively.

The impact of the weakening is also expressed through the integrated lithospheric strength, which is calculated for each scenario as the depth integral of yield stress down to the lithosphere thickness defined by the 1300 °C isotherm. Unsurprisingly, the highest integrated lithospheric strength is reached with a non-weakened lithosphere (Fig. 3a) at 21 x 10^{12} $N.m^{-1}$.

233 The lowest integrated lithospheric strength is reached with a whole lithosphere weakening
234 (Fig. 3e) at 8 x 10^{12} N.m^{-1}. Intermediate strengths are found with a brittle, entire crust and a
235 mantle weakening at 19, 18 and 11 x 10^{12} N.m^{-1}, respectively. The mantle weakening reduces
236 the integrated lithospheric strength more than 60%, versus ca. 10% with a brittle or entire
237 crust weakening. This major role of a weakened mantle on analytic yield stress profiles is one
238 of main result of Mazzotti and Gueydan (2017). The importance of investigating the
239 integrated lithospheric strength will be presented in section 3.
240

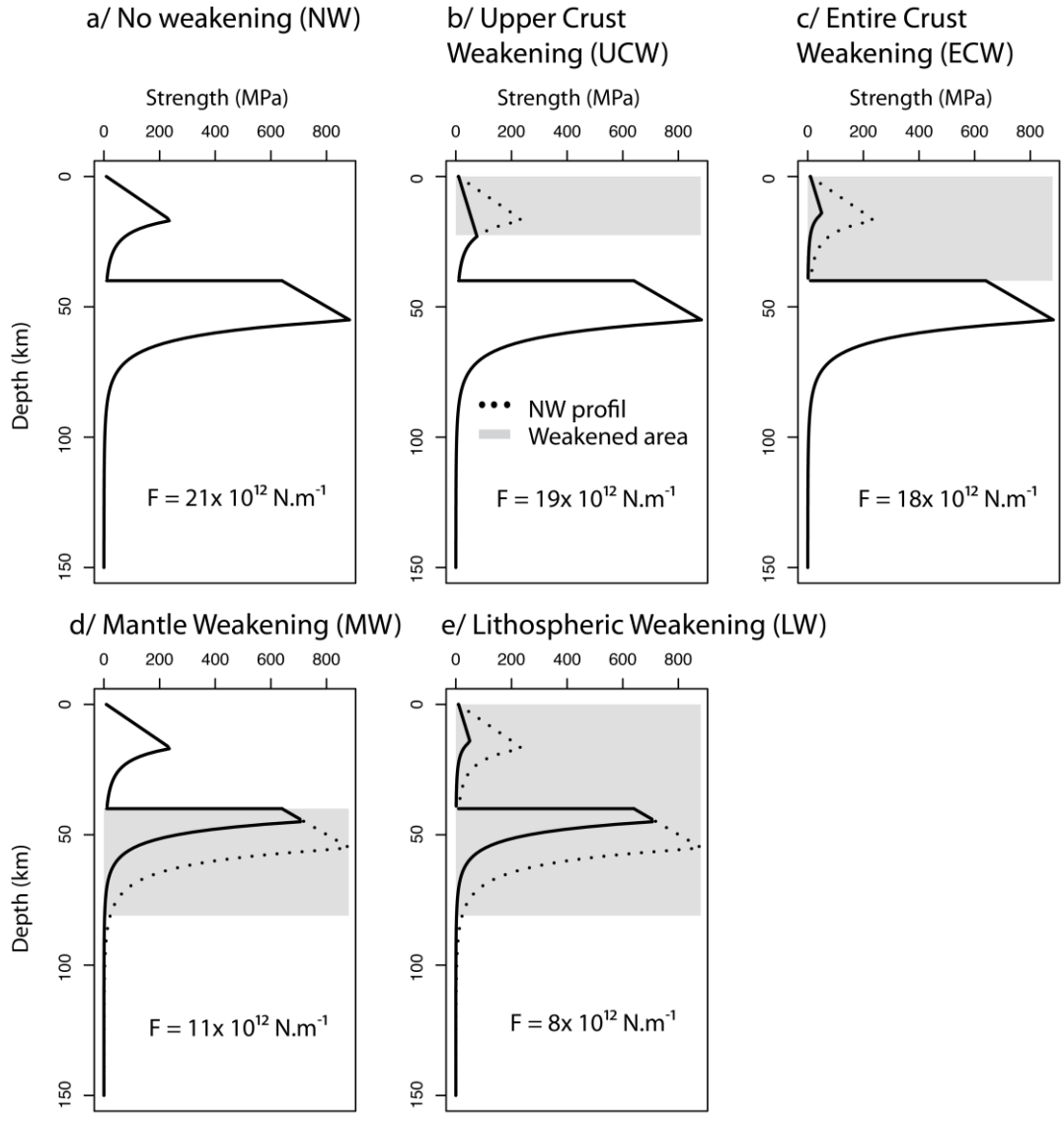

241

Figure 3. Theoretical yield stress profiles without and with weakening. Mohr-Coulomb criterion and dislocation creep law are used for brittle and ductile behavior, respectively. A weakening coefficient is used for brittle and ductile weakening (cf. text). Yield stress profiles calculated for various localizations of the weakened domain (grey area), with a uniform strain rate of 5.6 x 10^{-17} s^{-1}. F: integrated lithospheric strength assumed at equilibrium with net driving force.

2.2 Geometry and boundary conditions

We use the 2D numerical thermo-mechanical finite-element code ADELI (Hassani et al., 1997). The model integrates elastic, viscous and plastic behaviors. Our model is tuned to apply to a generic intraplate deformation zone represented by a lithosphere of 600 km length and 150 km thickness including a 40-km-thick crust (Fig. 4). It is discretized in 10 000 linear elements (triangles), with a node interspacing of ca. 4 km. The geotherm is uniform for the

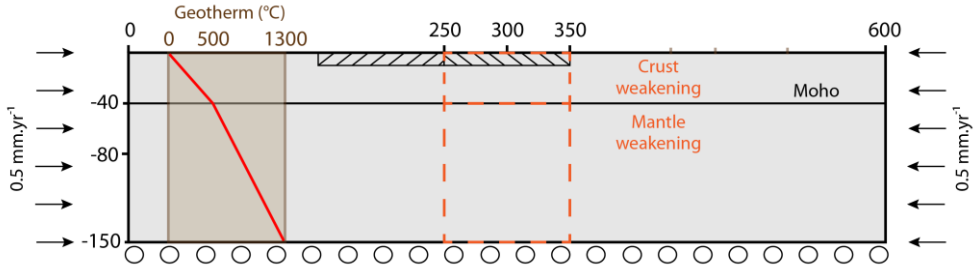

Figure 4. Geometry and boundary conditions of the elasto-visco-plastic thermo-mechanical model. Basal boundary condition: null vertical velocity and a free horizontal velocity. Lateral boundary condition: null vertical velocity and fixed horizontal velocity (e.g., 0.5 $mm.yr^{-1}$). Black numbers are distances (km). Weakened areas are delimited by orange dashed lines. The two hatched zones between 0 and 10 km depth indicate the two areas where upper crustal strain rate amplification factor is calculated (weakened over non-weakened area).

whole model and defined as linear gradients between the surface (0 °C), Moho, and base (1300 °C) temperatures. In continental intraplate domains, measured surface heat flow and geotherm models correspond to Moho temperatures varying between 400-500 °C in the coldest environments (e.g., Canadian Shied; Mareschal et al., 2000) and ca. 600 °C in milder settings (e.g., central USA; Zoback and Townend, 2001). As our models represent intraplate deformation zones, excluding cratons, we set the reference Moho temperature at 500°C. Higher Moho temperatures will be considered in section 5.1.

The models are constrained by a shortening velocity of 1 $mm.yr^{-1}$ (0.5 $mm.yr^{-1}$ on each side of the model), constant with depth. The impact of lower velocities (0.05, 0.1 and 0.5 $mm.yr^{-1}$), representative of the range of deformation rates in intraplate deformation zones, will be tested section 5.1. The base of the model is free horizontally and fixed in the vertical component. These boundary conditions define a displacement flow that converges towards the model center, with no strain rate concentration in the upper crust in the central region compared to the peripheries (see section 3). This ensures stable numerical results in the various tests. The kinematic conditions predefine the model bulk strain rate. Thus, in order not to provide strain rate results that are controled by the boundary conditions, we do not discuss the modeling results in terms of absolute strain rate values but rather as a normalized strain rate (relative to the predefined bulk). Similarly, we express the impact of structural inheritance on upper crustal deformation in terms of an amplification factor, i.e. the ratio of strain rate in the weakened region over that in a non-weakened region (calculated over two conterminous 100 x 10 km zones, cf. Fig. 4).

The chosen length of 100 km of the weakened area represents an approximation of the spatial extent of structural inheritance (for example, the paleo Iapetus rift, North America, or the Hercynian domain in western France including the South Armorican Shear Zone). Ductile

deformation leading to shear zones in the lower crust and lithospheric mantle in rift zones also appear to be spatially spread over 50-100 km (Gueydan et al., 2008). In our approach, we assumed that the weakening occurs homogeneously over the 100 km length. In other words, the structural inheritance is modeled as a weakened domain representing a distributed fault and shear zone system. Modeling a weakened domain allows representing any intraplate deformation zones, whereas modeling a complex fault system would be representative of one specific area.

3. Reference non-weakened model

Because of the velocity boundary conditions, the strain and stress values in our numerical models change with every time step. Figure 5a shows profiles of differential stress (second invariant J_2) of the model at various run times (0.3 – 7.8 Myr), compared with the steady-state yield stress analytic profile. The model differential stresses increase with each time step, until it becomes similar to the analytic yield stresses at. 7.8 Myr. Slight differences exist between the two for the brittle domains that can be attributed to the Drucker-Prager vs. Mohr-Coulomb parameterizations (cf. section 2.1.1). The modeled integrated lithospheric strength follows a similar pattern and reaches the analytic value (21×10^{12} N.m^{-1}) at 7.8 Myr.

Thus, model stress and strain vary with time, depending primarily on the imposed velocity boundary condition. In order not to depend on the imposed velocity, for which we only know the upper bound in intraplate deformation zones, we analyse the model results assuming that the lithosphere is at equilibrium between the integrated strength and a net force that corresponds to the combined effect of tectonic and other transient processes (cf. Zoback and Townend, 2001; Mazzotti and Gueydan, 2017). Estimations of tectonic forces range from 1 to 10×10^{12} N.m^{-1} (e.g., Forsyth and Uyeda, 1975; Copley et al., 2010). Transient processes

such as erosion or sedimentation pulses, or glacial isostatic adjustment can produce force increments about 1-2 x 10^{12} N.m^{-1} (Calais et al., 2010; Wu and Johnston, 2000; Wu and Mazzotti, 2007). Hereafter, we consider models associated with an integrated lithospheric strength and a net driving force of 6 x 10^{12} N.m^{-1}, which corresponds to a time run of 0.7 Myr (Fig. 5a). The impact of lower (3 x 10^{12} N.m^{-1}) and higher (10 x 10^{12} N.m^{-1}) forces will be tested section 5.1. As a result, our analysis corresponds to models at intermediate run times and differential stress profiles and not to model that have reached a steady state.

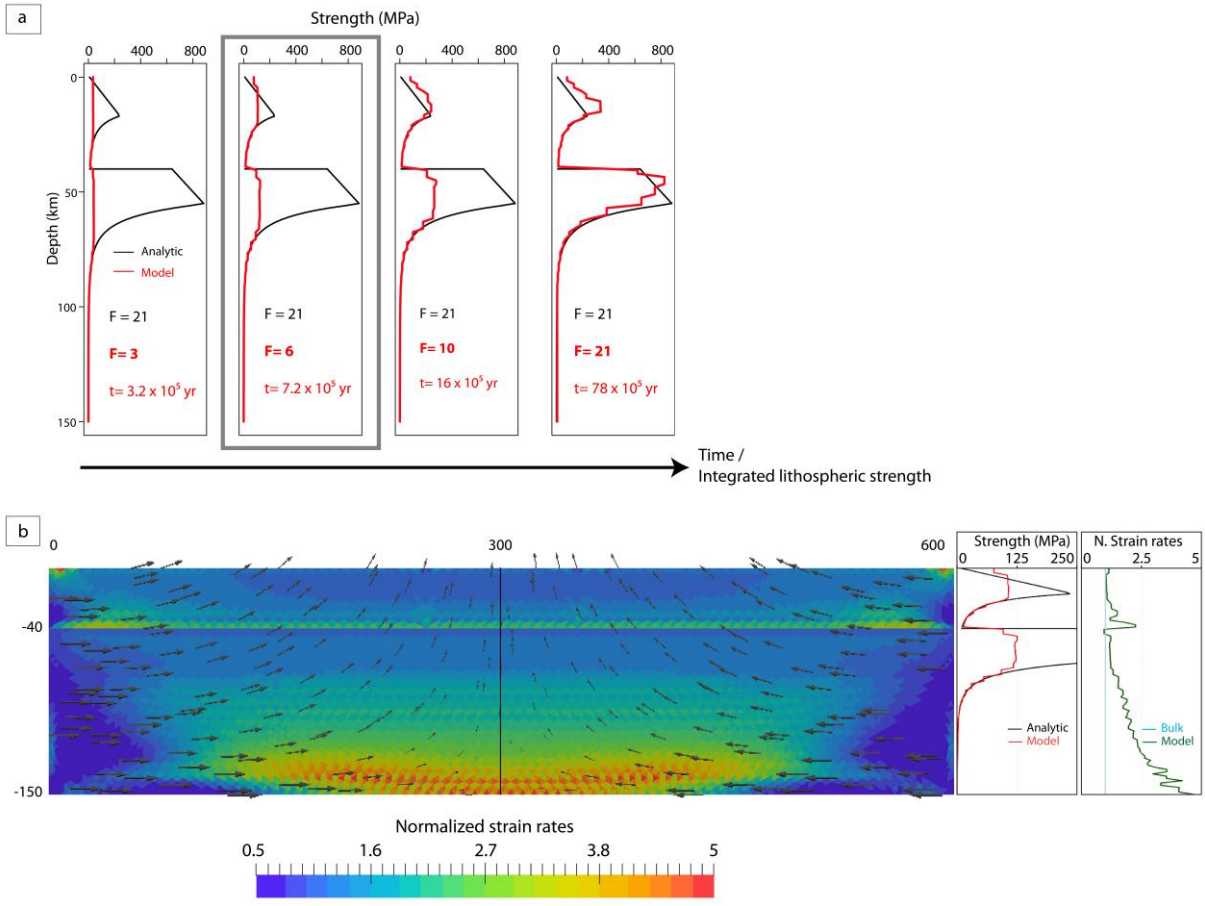

Figure 5. Reference model with no weakening. a/ Comparison of analytic steady-state yield stress (black) and model J2 stress (red). F: integrated lithospheric strength assumed at equilibrium with net driving force (x 10^{12} N.m^{-1}), t: time (yr). b/ Non-weakening model for a force F = 6x10^{12} N.m^{-1}. Background colours are normalized strain rates (relative to model bulk). Black vectors show the displacement field. Black numbers are distances (km). Right panels: analytic and model stress profiles and normalized strain rate profile located at model

328 center (vertical black line). Bulk line represents boundary condition mean strain rate (e.g.,
329 velocity of 1 mm.yr^{-1} over 600 km).
330
331 For this net driving force of 6 x 10^{12} N.m^{-1}, a major feature in our model is the
332 presence of large elastic layers (Fig. 5a) due to the slow stress build up. The presence of
333 elastic layer in the lithosphere for a non-steady state model is well established (e.g. Kuzsnir,
334 1991). For forces of (3 – 6) x 10^{12} N.m^{-1}, elastic layers are preserved in the upper-middle crust
335 and in the upper lithospheric mantle. The thickness of the elastic layers decreases with time as
336 differential stress build up to reach brittle and ductile yield stress values. For a force of 10 x
337 10^{12} N.m^{-1}, the elastic layer has disappeared in the crust. Whole lithosphere near-failure
338 equilibrium occurs for a force of 21 x 10^{12} N.m^{-1}.
339 The overall deformation pattern of the non-weakened model is presented in Figure 5b.
340 In order not to depend on the imposed boundary velocity and to help visualisation, we present
341 the strain rates as normalized to the overall model bulk strain rate (boundary velocity divided
342 by the model length). High strain rates are concentrated in two main shear zones: just above
343 the Moho (due to the weak ductile stress of quartz at the lowermost-crust temperature) and at
344 the base of the lithosphere (due to the vertical-fixed base of the model). Conversely, low
345 strain rates occur in domains of high differential stress in the upper crust and upper
346 lithospheric mantle. The two elastic layers seen in Figure 5a are characterized by low strain
347 rate values. The thickness of the elastic layers is ~18 km in the upper-middle crust and ~27
348 km in the upper lithospheric mantle. As discussed section 2.2, the model presents no strain
349 rate concentration in the upper crust in the central region, compared to the peripheries (Fig.
350 5b). This point is important for the interpretations of the following models where the
351 weakened domain is located in the center. The high strain rates located on each upper corners
352 of the model are due to the velocity boundary condition. However, the strain rate

amplification factors are calculated near the center of the model (see Figure 4) and are thus not affected by these boundary effects.

4. Weakened models for a net driving force of 6 x 10^{12} N.m^{-1}

In the following, we assess the effect on upper crustal strain rate amplification factor of weakened zones in various locations (from upper crust to whole lithosphere) for a given amount of weakening ($\varepsilon = 2$), geotherm (T_M = 500 °C) and net driving force (F = 6 x 10^{12} N.m^{-1}). The models are shown in Figure 6 and, for each model, the upper crustal strain rate amplification factor is shown Figure 7 with respect to the reference non-weakened model.

4.1 Upper Brittle Crust Weakening (UCW)

With reduced friction coefficient, the strain rate amplification factor in the uppermost crust (strain rate ratio in weakened over non-weakened area) induced by the weakened upper crust is about a factor of 4 (Fig. 7). The strain rates concentrate in two bands on each side of the weakened area (Fig. 6a), which correspond to first-order to the Coulomb frictional bands that tend to accommodate and localize the shortening across the weakened upper crust. The maximum differential and yield stress in the weakened crust drop from ~125 MPa to ~75 MPa. Those two values correspond to the elastic differential stress and to the weakened brittle yield stress, respectively. Brittle weakened crust implies that yield stress is reached in the whole crust leading to the disappearance of the elastic layer in the weakened zone.

The strain rate concentration in the upper crust weakening impact the whole lithosphere profile. In the lower crust, strain rates increase compared to the reference non-weakened model due to stress concentration in the weakened upper-middle crust. In contrast,

strain rates decrease in the lithospheric mantle. The presence of the weakened upper crust creates a reorganization of the displacement field, leading to a reorganization of stress and strain rates. Because the boundary conditions prescribed the overall strain rate in the model, a local increase of the strain rates has to be balanced by a local decrease elsewhere in the model. This process explains also the reduced upper crustal strain rates directly outside the weakened area (ratio ca. 0.5 – 0.6).

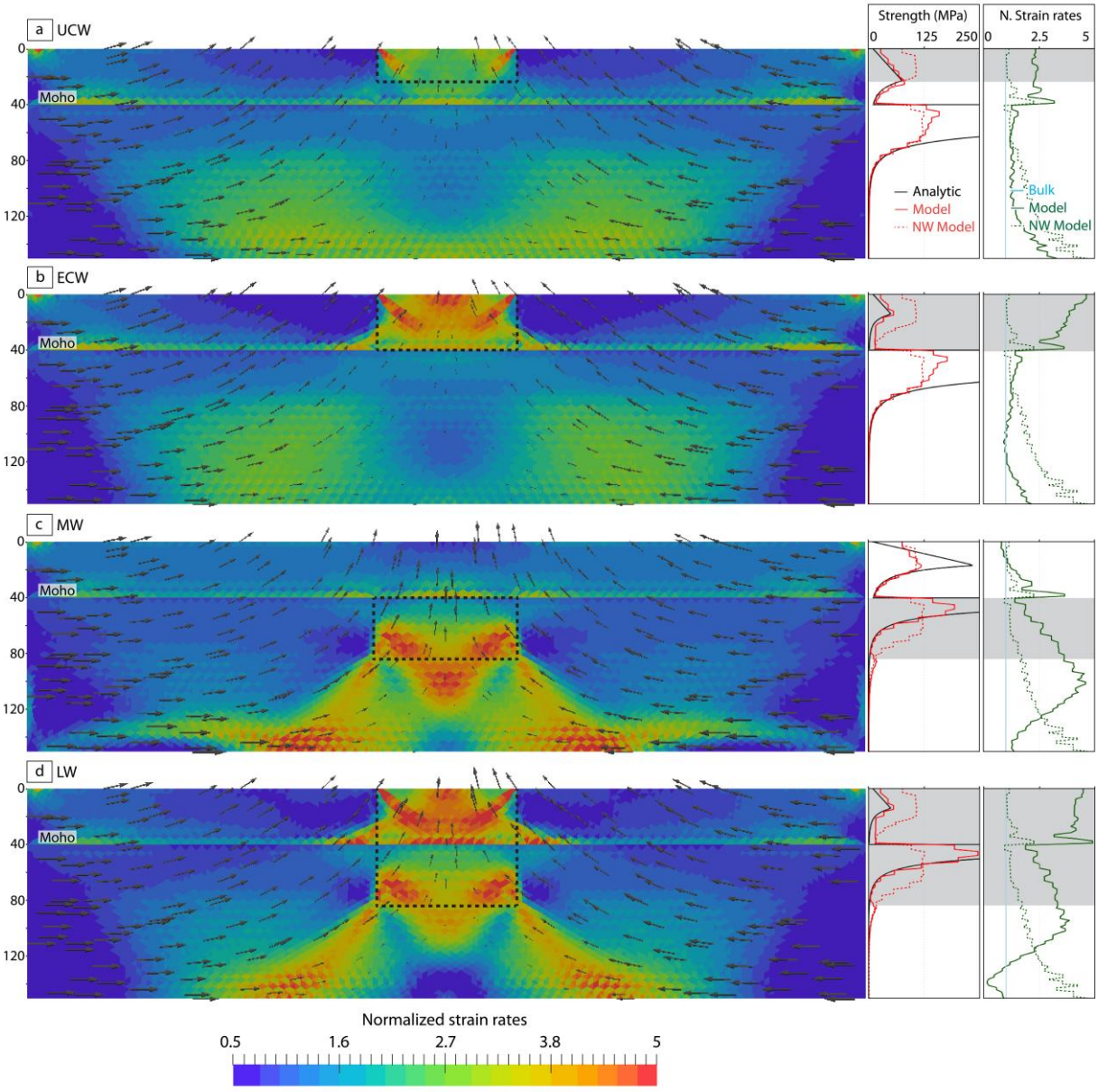

Figure 6. Models with weakening for a force of 6 x 10^{12} N.m^{-1}. Legend as Fig. 5. Dash lines in model and grey shaded areas in profiles show weakened areas. NW profile: reference non-weakening profile (Fig. 5b).

4.2 Entire Brittle and Ductile Crust Weakening (ECW)

With an entire crust weakened, the amplification factor of the upper crustal strain rate is about a factor of 6.6 (Fig. 7). The concentrated strain rates are mostly localized in three specific zones (Fig. 6b): (1) the two Coulomb bands on each side of the weakened area, which have propagated in depth and connected to the lower crust; (2) a shear zone at the Moho; and (3) a major brittle zone at the surface and center of the weakened area. The latter is not seen on the UCW model. The localized strain rate zones imply lateral variations of upper crustal strain rates. The major feature of the ECW model is that ductile weakening in the lower-middle crust significantly impacts the upper crustal strain rate concentration and amplification factor. Ductile weakening involves reduced differential stresses and larger strain rates (Eqs. 3-4) in the lower-middle crust. Compared to brittle weakening alone (Fig. 6a), the upper crustal strain rate is amplified by a factor of 2. This strong mechanical coupling between brittle and ductile layers is highlighted in studies investigating the role of each deformation mechanisms (i.e. brittle failure and viscous flow) in localized or distributed fracturing (e.g., Schueller et al., 2005, 2010).

4.3 Ductile Mantle Weakening (MW)

As seen section 2.1.2, only the lithospheric mantle with a temperature lower than 800°C is weakened, resulting in non-weakened lower lithosphere. Surprisingly, weakening of

410 the lithospheric mantle results in a reduction of upper crustal strain rate by a factor of 0.9
411 (Fig. 7). The displacement field associated with the enhanced mantle flow towards the weak
412 domain leads to the development of major shear bands in the lower part of the weakened
413 mantle and in the non-weakened mantle to accommodate the localized flow. More
414 specifically, the strain rates are localized on each side of the lower weakened part and in shear
415 zones from the weakened mantle to the base of the lithosphere (Fig. 6c). The weakened
416 mantle also creates a minor shear zones at the Moho. Despite the strong weakening in the
417 upper lithospheric mantle, the elastic layer is still present in the uppermost part of the
418 weakened mantle (40 – 60 km depth). This elastic layer prevents the stress propagation from
419 the mantle to the surface, explaining the absence of high strain rates in the crust.

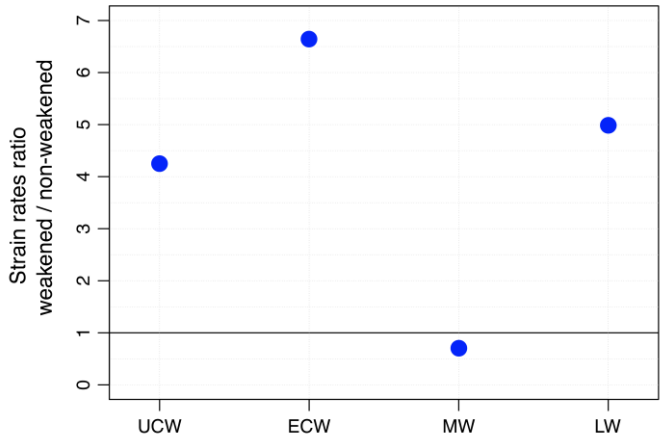

420

421 **Figure 7. Upper crustal strain rate amplification factor for five weakening scenarios**.
422 UCW: Upper Crust Weakening, ECW: Entire Crust Weakening, MW: Mantle Weakening and
423 LW: Lithosphere Weakening. Amplification factor expressed as ratio of average strain rate
424 inside weakened area over non-weakened area (cf. Fig. 4).

425

426 ***4.4 Brittle and Ductile Lithospheric Weakening (LW)***

427

428 The model with whole lithosphere weakening combines the high upper crustal strain
429 rate impact of the entire crust weakening and the low upper crustal strain rate impact of the

mantle weakening (Fig. 6d). The weakened lithosphere area induces an amplification factor of the upper crustal strain rate by a factor of 5 (Fig. 7). Higher displacements in the weakened domain lead to a major shear zones in the lower crust. This induces that the strain rate is slightly higher in the lower weakened crust than with the entire crust weakening (fig 6b).

5. Parametric study

In order for our models to be applied to any intraplate deformation zones, the impact of five major parameters (i.e. the velocity boundary condition, the crustal rheology, the amount of weakening, the net driving force, and the geotherm) will be tested separately. We investigate the influence of each parameter for the five scenarios of weakening localization. We pay specific attention to the lithospheric mechanical behavior related to the mantle elastic layer and to the mechanical coupling between the mantle, the ductile crust and the brittle crust.

5.1 Parameters sensitivity

We test the impact of the velocity boundary condition using three values (0.05; 0.1 and 0.5 $mm.yr^{-1}$, in addition to 1 $mm.yr^{-1}$ in the reference models) representative velocities of intraplate deformation zones (Figure 8a). Lower velocities display higher amplification factors, indicating a higher impact of structural inheritance. Changing the velocity boundary condition affects the amplification factors because we consider models for a given net driving force. Thus, lower boundary velocities imply lower average strain rates, promoting viscous versus elastic behaviors. Nevertheless, the amplification factors remain of the same order of magnitude in all experiments, varying from 1 – 7 in the reference models (velocity of 1

mm.yr^{-1}) to 1 –15 in the slowest models (velocity of 0.05 mm.yr^{-1}). The five weakening scenarios maintain the same deformation features with different velocities, e.g. a lower LW model amplification factor compared to the ECW model. This is due to the stability of the lithosphere rheological stratification with different velocity boundary conditions (see Appendix). For instance, the elastic layer is preserved over the same depth range of the upper part of the weakened mantle for all tested velocity boundary conditions, with only limited thinning with low velocity boundary condition. The impact of weakening on strain concentration is then linked to minor changes as the thickness of the elastic layer in the upper part of the weakened mantle decreases. Thus, the velocity boundary conditions do not significantly affect the model results and amplification factors, indicating, to first order, a linear scaling with the velocities.

To investigate the impact of crustal rheology, we consider a strong crust composed of granulite (dislocation creep parameters A = 1.4x10^{4} Pa^{-n}s^{-1}, Q = 445 J.mol^{-1}, n = 4.2; Wilks and Carter, 1990) instead of the quartz rheology used in the reference models (Fig. 8b). This provides, to first order, upper and lower limits on the rheology impact on upper crustal strain rate concentration. Compared to the quartz models, the amplification factor is significantly

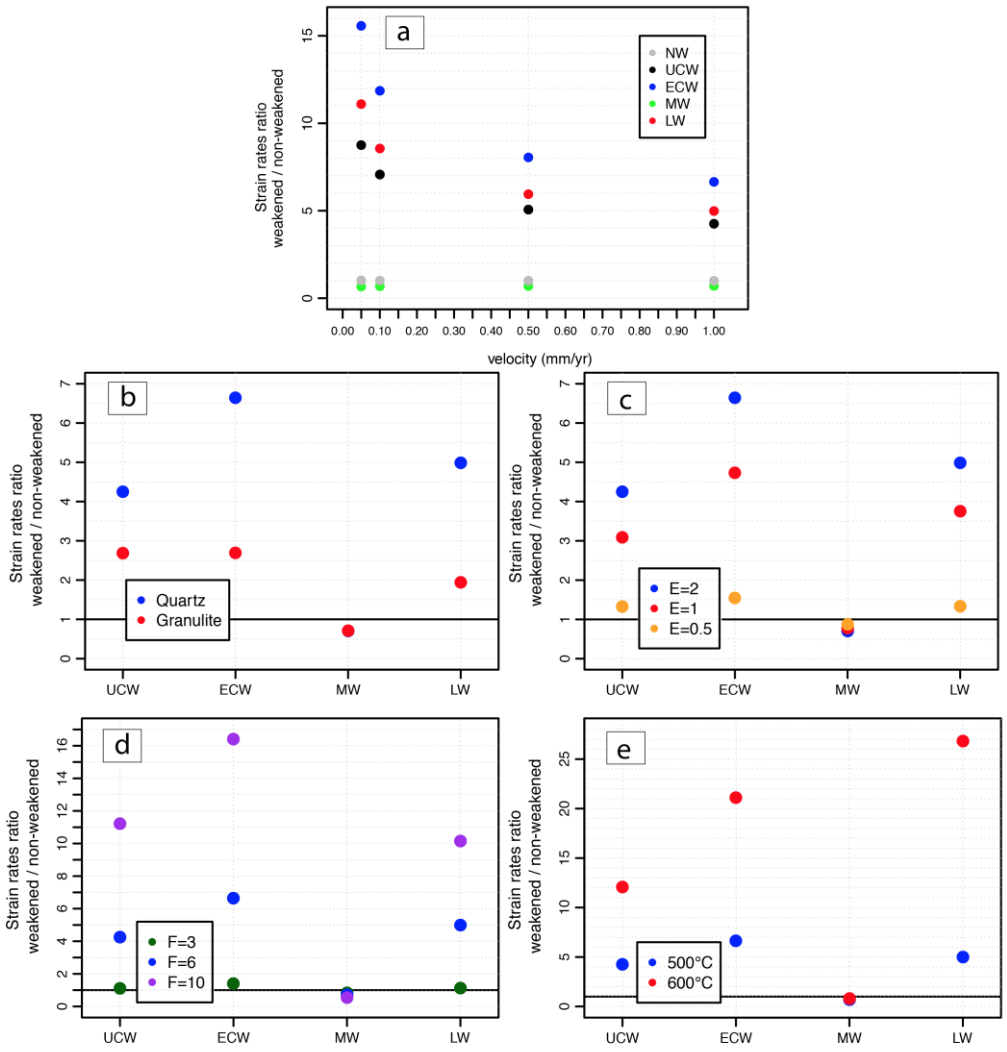

Figure 8. Parametric analysis of upper crustal strain rate amplification factor.

Amplification factors are calculated for different (a) velocity boundary conditions, (b) crustal rheology (granulite vs. quartz), (c) amount of weakening (E: inherited strain), (d) net driving force and (e) geotherm (given as Moho temperature). Blue circles for (b), (c), (d) and (e) are reference amplification factors shown Figure 7. Note different representation between (a) and (b – e).

smaller for all granulite models (down to factors of 2 – 2.7), except for the MW model (factor of 0.9). In the weakened area, the strain rate concentration is similar (two bands) for both rheologies but with lower values for the granulite. The granulite rheology implies a highest

yield stress, which results in (1) strain rates that are lower over the lithosphere column and (2) brittle failure occuring in the whole crust for both UCW and ECW models, leading to similar strain rate amplification factors.

The inherited finite strain in a structural inheritance domain controls the amount of weakening. In the reference cases, we assumed a high finite strain of 2 as representative, for example of a mature rift with lithospheric-scale paleo-structures (Musacchio et al., 1997). Figure 8c presents the impact of lower finite strains of 1 and 0.5 on the upper crustal strain rate amplification factors. Reducing the finite strain reduces the upper crustal strain rate ratios for all models (except the MW model) down to factors of 3 – 5 for a finite strain of 1 and 1 – 1.5 for a finite strain of 0.5. The strain rate concentration in the weakened area is similar but with lower strain rate values as we decrease the finite strain. With a low finite strain, the models for the five scenarios tend toward those of the NW model.

Variations of the net driving force change elastic layer thickness and thus the upper crustal strain rate concentration (see section 3). We quantify the impact on the upper crustal strain rate amplification factors of net driving forces of 10×10^{12} N.m^{-1} and 3×10^{12} N.m^{-1} (vs. reference value of 6×10^{12} N.m^{-1}, Fig. 8d). For a force of 10×10^{12} N.m^{-1}, the ratios increase for all models (except the MW model) reaching 16.5 for the ECW model. Because of the strain rate adjustment process, the upper crustal strain rates surrounding the weakened area decrease while they increase in the weakened area. This implies a higher weakened over non-weakened ratio for a force of 10×10^{12} N.m^{-1}. For a force of 3×10^{12} N.m^{-1}, the ratio decreases for all models (except the MW model) down to factors of 1 – 1.5. The mantle flow is slower, leading to a lower concentration of strain rates in the weakened area. Thus, for a net driving force of 3×10^{12} N.m^{-1}, weakening has no significant impact on upper crustal strain rate amplification factors.

Finally, we test a geotherm defined by T_M = 600°C (vs. reference value of 500°C) in order to quantify the impact of temperature on upper crustal strain rate amplification factors (Fig. 8e). The upper crustal strain rate ratio increases for all models up to factors of 21 – 27 (except the MW model). The highest amplification factor difference is with the LW model. For T_M = 600°C, the differential stresses in the whole weakened lithosphere are significantly lower than with a T_M = 500°C. More particularly, ductile flow occurs in the whole upper lithospheric mantle, suppressing the elastic layer preserved with a T_M = 500°C. As a consequence, the mechanical crust-mantle coupling is stronger, leading to an increase of the upper crustal strain rate amplification factor.

5.2 Summary of amplification factor parameters variability

The parameter that has the highest impact on upper crustal strain rate amplification factor is the geothem. A relatively high Moho temperature (T_M = 600°C) leads to maximal amplification factors of 21 – 27. A high net driving force (10 x 10^{12} $N.m^{-1}$) also promotes high amplification factors of 11 – 17. These two parameters play a major role in upper crustal strain rate concentration only for a high amount of weakening (i.e. a finite strain of 2). The role of the weakening is fundamental to produce high concentration and amplification factors. The parameter that has the lowest impact on the upper crustal amplification factor is the crustal rheology. At first order, the velocity imposed to the model does not influence significantly the amplification factor. Investigating the interactions between these parameters and their combined impact on strain rate concentration and amplification factor will require further dedicated models.

6. Discussion

6.1 Impact of weakened areas on intraplate strain rates and seismicity levels

On the basis of the numerical models and the parametric tests, we propose a conceptual model that relates, to first order, the structural inheritance with present-day strain rate and seismicity concentration in intraplate deformation zones (Fig. 9). The main objective is to present the possible variations of lithospheric structure linked to high or moderate strain rate concentration. Because earthquakes are not directly modeled in our study, we make the simple assumption that seismicity levels can be directly related to strain rate concentrations.

Moderate strain rate amplification factors (ca. 4 – 10) and seismicity levels may be associated with a high inherited weakening (ε >1) in the crust only or in the whole lithosphere, a moderate or high net driving force (6 – 10 x 10^{12} N.m^{-1}), or a medium geotherm ($500°C \leq T_M < 600°C$). Examples of this moderate case could be the Appalachian thrust nappes, which may be associated with upper crust weakening but not lithospheric inheritance, or whole lithosphere weakening and a cold geotherm (e.g., parts of the Iapetus rift close to the Canadian Shield). In contrast, the Hercynian domain including the South Armorican Shear Zone (western France) may have preserved lithospheric inheritance and could be explained by moderate net driving force.

On the other hand, higher strain rate amplification factors up to 15 – 30, and thus potentially higher seismicity levels, can be reached in domains of crust weakening associated with high net driving force (10 x 10^{12} N.m^{-1}) or in domains of whole lithosphere weakening and mild geotherms (T_M = 600°C), as shown Fig. 9. This may be the case of specific regions of the Iapetus Rift (e.g., St Lawrence Valley, New Madrid seismic zone).

The structure of the lithosphere (i.e. the presence of structural inheritance and the associated weakened rheology) is representative of a long-term state. The first-order

explanation linking the presence of seismicity with models of different lithospheric structures (Fig. 9) assumes that the seismicity is also representative of a long-term behavior. This raises the question of seismic concentration as long-term or transient (temporal clusters). Long-term seismic concentration could be attributed to lithospheric structures, whereas transient seismic concentration could involve other processes localizing the strain rates. To address this issue, we compare modeled and observed strain rate amplification factors in the following section.

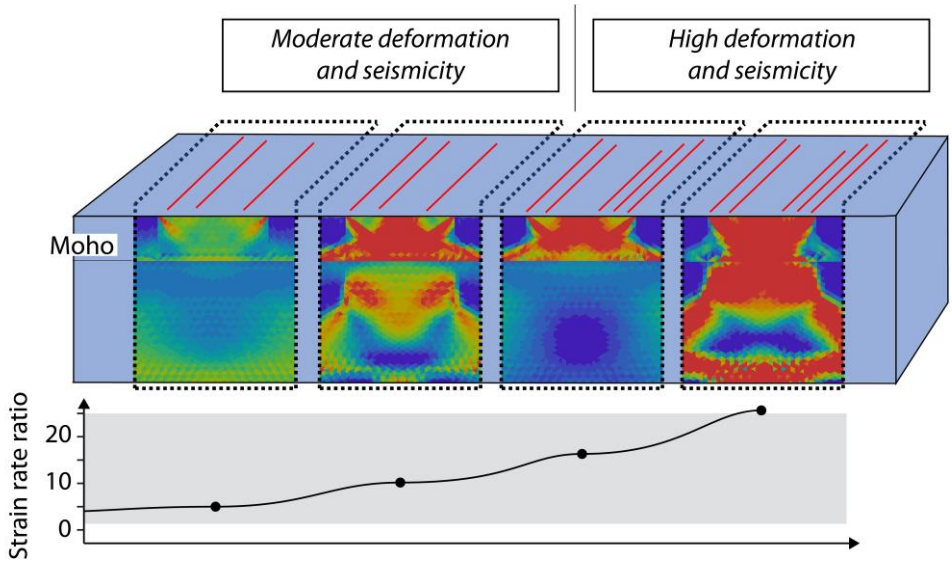

Figure 9. Conceptual model relating structural inheritance with upper crustal strain rate and seismicity concentration in intraplate deformation zones. Red lines show schematic fault traces. Modeling results represent from left to right: UCW model in Fig. 6, model of lithospheric weakening with F = 10 x 10^{12} N.m^{-1}, model of crustal weakening with F = 10 x 10^{12} N.m^{-1} and model of lithospheric weakening with Moho Temperature of 600°C. Lower curve shows variations of upper crustal strain rate amplification factor for each model. Amplification factors of 4-10 and 15-30 are representative of moderate and high deformation and seismicity, respectively. Grey shaded area represents seismic and GPS strain rate amplification factors observed at large spatial scale (cf. Table 1).

6.2 Comparison between modeled and observed strain rate amplification factors

Intraplate strain rates, more particularly in non-weakened areas, are challenging to measure because of their low magnitude. Estimations of strain rate amplification factors (i.e. weakened over non-weakened strain rate ratios) can be made in the central and eastern North America using published GPS and seismicity data (assuming that the seismic catalog is representative of a long-term strain rate). Table 1 presents these amplification factors calculated for regions of large (several hundred kilometers) and small (50-100 km) spatial scales. The large spatial scale strain rates are calculated in (i.e. weakened area) and around (i.e. non-weakened area) the Saint Lawrence Valley. The regions IRM, LAB and COC in Table 1 are three subsections of the St Lawrence Valley (see Mazzotti and Adams, 2005). Amplification factors range from 2 to 25 with a good coherence between those calculated by GPS and seismicity. The smaller spatial scale strain rates are calculated in specific seismically active areas: New-Madrid, Charlevoix, Lower St Lawrence (BSL) and Montréal. GPS amplification factors range from 12 to 200. Seismic amplification factors range from 275 to 7000.

We obtain a reasonable agreement between modeled strain rate amplification factors and large scale observed amplification factors (roughly factors of 5 – 30). If the ergodic hypothesis is verified (i.e. the system has the same behavior averaged over time and averaged over space), strain rates calculated on high spatial scale are representative of a long-term deformation. Modeled strain rate amplification factors should be representative of a long-term deformation and seismicity level. In this framework, the local seismic zones of Charlevoix, Montréal and New Madrid could be associated with temporal clusters of seismicity.

However, a direct comparison between the modeled and local (small-scale) observed strain rate amplification factors is not easy to make. A first explanation of the discrepancy is that our models lack the complexity to be compared with natural cases. Secondly, although

599 the differences between large and small-scale amplification factors are significant, significant
600 uncertainties remain. Main uncertainties on observed strain rates are: (1) those specific to the
601 strain rate calculation method (see references in Table 1); (2) the differences between large
602 and small-scale amplification factors are significant for seismic amplification factors but not
603 for GPS amplification factors; (3) the background in Table 1 (i.e. the non-weakened zone) is
604 not the same for all calculated ratios. To address this issue, numerical models representing
605 each specific area are required. Complexity in the lithospheric structure and local processes
606 should be considered.

Region	Seismic strain rate ratio	GPS strain rate ratio
Large scale region:		
SLV /background	25 [a]	2 - 11 [c]
IRM / background	24 [b]	
LAB / background	10 [b]	
COC / background	5 [b]	
Small scale region:		
New Madrid /background	7000 [d]	
Charlevoix / background	6350 [b]	12 [c] - 200 [e]
Montréal / background	277 [b]	13 [c]
BSL / background	275 [b]	

607

608 **Table 1. Strain rate amplification factors from seismicity and GPS observations**
609 (weakened area over non-weakened area strain rate ratios). Large and small scale regions are
610 about 500 – 1000 and 10s – 100s km scale, respectively. SLV: Saint Lawrence Valley, IRM:
611 Iapetus Rift Margin, BSL: Bas Saint Laurent, LAB: southern LABrador and COC:
612 COChrane. All these regions are situated along the St Lawrence Valley (Eastern Canada). a:
613 Mazzotti and Gueydan (2017) and references therein, b: Mazzotti and Adams (2005), d:
614 Anderson (1986), c: Tarayoun et al. (2018) and e: Mazzotti et al. (2005).

615

616 **7. Conclusion**

The role of structural inheritance, proposed as a strain concentrator, is a key element to understand the current strain rate and seismicity concentration in intraplate deformation zones. In this study, we quantified the impact of the structural inheritance (i.e., presence of large paleo-tectonic structures), through 2D numerical modeling of weakened domains at different locations in the lithosphere. More specifically, we have quantified the amplification factor of upper crustal strain rates associated with structural inheritance. Our analysis yields three main conclusions:

(1) Lithospheric structural inheritance has a major impact on the concentration and amplification of upper crustal strain rates. Amplification factors range from 1 to 27, depending on the assumed rheology, geotherm, net driving force, and amount of inherited weakening (Fig. 8). High upper crustal deformation is accentuated with a weak rheology, a high amount of weakening (i.e. a high inherited finite strain), a high net driving force and a mild geotherm.

(2) The concentration of upper crustal strain rate varies strongly depending on the location of the weakened area in the lithosphere. Weakened zones with the highest impact are the entire crust and the whole lithosphere for a Moho temperature at 500°C and 600°C, respectively. Lithospheric mantle weakening has no impact for a cold geotherm (T_M = 500°C) and only accentuates the upper crustal deformation very slightly at milder geotherm (T_M = 600°C).

(3) Modeled strain rate amplification factors are in reasonable agreement with those calculated from GPS and seismicity data at large spatial scales (several 100s km), thus potentially representative of a long-term deformation (Table 1).

A major feature of our models is the presence of preserved elastic layer in the upper lithospheric mantle for low Moho Temperature (i.e. 500°C). This elastic layer has a strong

642 impact on upper crustal strain rate concentration in a way that it tends to prevent high
643 amplification factors. Our innovative modeling approach, coupling velocity boundary
644 conditions and net force constraints, allows highlighting the presence of this preserved elastic
645 layer, with significant impact on the mechanical behavior of the lithosphere and potentially, in
646 the long term, on seismicity and seismic hazard characterization in intraplate deformation
647 zones.
648
649 **Acknowledgements**
650 We thank Walter D. Mooney and two anonymous reviewers for their comments that helped to
651 improved and clarify the manuscript. Discussions with Jean Chéry are gratefully
652 acknowledged. USGS National Earthquake Information Center (NEIC) can be found at:
653 https://earthquake.usgs.gov/data/scr_catalog.php. This work was supported by the French
654 Agence National de la Recherche through grant ANR-12-CHEX-0004-01 (DefDyCor) to
655 SM.
656
657 **References**
658
659 Adams, J., & Basham, P.W. (1991). The seismicity and seismotectonics of eastern Canada. In
660 D. B. Slemmons et al., *Neotectonics of North America, Decade Map* (Vol. 1, pp. 261-
661 276), Geological Society of America Boulder, Colorado.

662 Anderson , J. G. (1986). Seismic strain rates in the central and eastern United States, *Bulletin*
663 *of the Seismological Society of America*, 76, 273-290.

664 Boneh, Y., Wallis, D., Hansen, L. N., Krawczynski, M. J., & Skemer P. (2017). Oriented
665 grain growth and modification of 'frozen anisotropy' in the lithospheric mantle, *Earth*

666 *and Planetary Science Letters*, 474, 368-374.
667 https://doi.org/10.1016/j.epsl.2017.06.050

668 Byerlee, J. (1978). Friction of Rocks. In J.D. Byerlee, & M. Wyss, (Eds), *Rock Friction and*
669 *Earthquake Prediction* (pp. 615-626). Contributions to Current Research in
670 Geophysics (CCRG), vol 6. Birkhäuser, Basel. https://doi.org/10.1007/j978-3-0348-
671 7182-2_4

672 Calais, E., Freed, A. M., Van Arsdale, R., & Stein, S. (2010). Triggering of New Madrid
673 seismicity by late-Pleistocene erosion, *Nature*, 466, 608-611.
674 https://doi.org/10.1038/nature09258

675 Chéry, J., Zoback, M. D., & Hassani, R. (2001). An integrated mechanical model of the San
676 Andreas fault in central and northern California, *Journal of Geophysical Research*,
677 106, 22,051-22,066. https://doi.org/10.1029/2001JB000382

678 Copley, A., Avouac, J.-P., Royer, J.-Y. (2010). India-Asia collision and the Cenozoic
679 slowdown of the Indian plate: implications for the forces driving plate motions,
680 Journal of Geophysical Research, 115, 1-14. https://doi.org/10.1029/2009JB006634

681 Coppersmith, K. J., Johnston, A. C., Metzger, A. G., & Arabasz, W. J. (1987). Methods for
682 assessing maximum earthquakes in the central and eastern United States, Electric
683 Power Research Institute, working report EPRI RP2556-12, pp. 312.

684 Forsyth, D., & Uyeda, S. (1975). On the relative importance of the driving forces of plate
685 motion, *Geophysical Journal International*, 43, 163-200.
686 https://doi.org/10.1111/j.1365-246X.1975.tb00631.x

687 Gorczyk, W., Hobbs, B., & Gerya T. (2012). Initiation of Rayleigh-Taylor instabilities in
688 intra-cratonic settings, *Tectonophysics*, 514-517.
689 https://doi.org/10.1016/j.tecto.2011.10.016.

690 Grollimund, B., & Zoback, M. D. (2001). Did deglaciation trigger intraplate seismicity in the
691 New Madrid seismic zone ?, *Geology*, 29, 175-178. https://doi.org/10.1130/0091-
692 7613(2001)029<0175:DDTISI>2.0.CO;2

693 Gueydan, F., Leroy, Y. M., Jolivet, L., & Agard, P. (2003). Analysis of continental midcrustal
694 strain localization induced by microfracturing and reaction-softening, *Journal of*
695 *Geophysical Research*, 108, 175-178. https://doi.org/10.1029/2001JB000611

696 Gueydan, F., Morency, C., & Brun, J-P. (2008). Continental rifting as a function of
697 lithosphere mantle strength, *Tectonophysics*, 460, 83-93.
698 https://doi.org/10.1016/j.tecto.2008.08.012

699 Gueydan, F., Précigout, J., & Montési, L. G. J. (2014). Strain weakening enables continental
700 plate tectonics, *Tectonophysics*, 631, 189-196.
701 https://doi.org/10.1016/j.tecto.2014.02.005

702 Hassani, R., Jongmans, D., & Chéry, J. (1997). Study of plate deformation and stress in
703 subduction processes using two-dimensional numerical models, *Journal of*
704 *Geophysical Research*, 102, 17951-17965.

705 Hirth, G., & Kohlstedt, D. (2003). Rheology of the uppermantle and the mantle wedge : a
706 view from the experimentalists. In J. Eiler, (Ed), *Inside the Subduction Factory* (138,
707 pp. 83-105).

708 Holdsworth, R. E. (2004). Weak faults – rotten cores, *Science*, 303, 181-182.
709 https://doi.org/10.1126/science.1092491

710 Illies, J. H. (1972). The Rhine graben rift system-plate tectonics and transform faulting,
711 *Geophysical Surveys, 1*, 27-60.

712 Jégouzo, P. (1980). The South Armorican Shear Zone, *Journal of Structural Geology, 2*, 39-
713 47.

714 Johnston, A. C. (1989). The seismicity of "stable continental interiors". In S. Gregersen, & P.
715 W. Basham, (Eds), *Earthquakes at North-Atlantic Passive Margins: Neotectonics and*
716 *Postglacial Rebound* (pp.299-327). Kluwer Academic Publishers, Dordrecht, The
717 Netherlands.

718 Kenner, S. J., & Segall, P. (2000). A Mechanical Model for Intraplate Earthquakes :
719 Application to the New Madrid Seismic Zone, *Science,* 289, 2329-2332.
720 https://doi.org/10.1126/science.289.5488.2329

721 Kumarapeli, P. S., & Saull, V. A. (1966). The St. Lawrence Valley system: a North American
722 equivalent of the East African Rift Valley system, *Canadian Journal of Earth*
723 *Sciences*, Vol. 3.

724 Kusznir, N. J. (1991). The distribution of stress with depth in the lithosphere : thermo-
725 rheological and geodynamic constraints. In R. B. Whitmarsh, (Ed), *Tectonic Stress in*
726 *the Lithosphere* (pp. 95-107). Royal Society, London.

727 Luan, F. C., & Paterson, M. S. (1992). Preparation and deformation of synthetic aggregates of
728 quartz, *Journal of Geophysical Research*, 97, 301-320.
729 https://doi.org/10.1029/91JB01748

730 Mareschal, J. C., Jaupart, C., Gariépy, C., Cheng, L. Z., Guillou-Frottier, L., Bienfait, G., &
731 Lapointe, R. (2000). Heat flow and deep thermal structure near the southeastern edge
732 of the Canadian Shield, *Canadian Journal of Earth Sciences*, 37, 399-414.

733 Mazzotti, S., & Adams, J. (2005). Rates and uncertainties on seismic moment and
734 deformation in eastern Canada. *Journal of Geophysical Research: Solid Earth*, 110,
735 B09301. https://doi.org/10.1029/2004JB003510

736 Mazzotti, S., James, T. S., Henton, J., & Adams, J. (2005). GPS crustal strain, postglacial
737 rebound, and seismic hazard in eastern North America: The Saint Lawrence valley

738 example. *Journal of Geophysical Research*, 110, B11301.
739 https://doi.org/10.1029/2004JB003590

740 Mazzotti, S., & Gueydan, F. (2017). Control of tectonic inheritance on continental intraplate
741 strain rate and seismicity, *Tectonophysics*. https://doi.org/10.1016/j.tecto.2017.12.014

742 Mooney, W. D., Laske, G., & Masters, G. (1998). CRUST 5.1 : A global crustal model at 5° x
743 5°, *Journal of Geophysical Research*, 103, 727-747.

744 Musacchio, G., Mooney, W. D., Luetgert, J. H., & Christensen, N. I. (1997). Composition of
745 the crust in the Grenville and Appalachian Provinces of North America inferred from
746 Vp/Vs ratios, *Journal of Geophysical Research*, 102, 15,225-15,241.
747 https://doi.org/10.1029/96JB03737

748 Owen, D. R. J., & Hinton, E. (1980). *Finite Element in Plasticity*. Pineridge Press Limited.

749 Précigout, J., & Gueydan, F. (2009). Mantle weakening and strain localization: Implications
750 for the long-term strength of the continental lithosphere, *Geology*, 37, 147-150.
751 https://doi.org/10.1130/G25239A.1

752 Regenauer-Lieb, K., & Yuen, D. A. (2003). Modeling shear zones in geological and planetary
753 sciences : solid- and fluid-thermal-mechanical approaches, *Earth-Science Reviews*, 63,
754 295-349. https://doi.org/10.1016/S0012-8252(03)00038-2

755 Schueller, S., Gueydan, F., & Davy, P. (2005). Brittle-ductile coupling: Role of ductile
756 viscosity on brittle fracturing, *Geophysical Research Letters*, 32.
757 https://doi.org/10.1029/2004GL022272

758 Schueller, S., Gueydan, F., & Davy, P. (2010). Mechanics of the transition from localized to
759 distributed fracturing in layered brittle-ductile systems, *Tectonophysics*, 484, 48-59.
760 https://doi.org/10.1016/j.tecto.2009.09.008

761 Schulte, S. M., & Mooney, W. D. (2005). An updated global earthquake catalogue for stable
762 continental regions: reassessing the correlation with ancient rifts, *Geophysical Journal*
763 *International*, 161(3), 707–721, https://doi.org/10.1111/j.1365-246X.2005.02554.x

764 Stein, S., & Mazzotti, S. (2007). Continental Intraplate Earthquakes: Science, Hazard, and
765 Policy Issues. The Geological Society of America, Special paper 425.

766 Sykes, L. R. (1978). Intraplate seismicity, reactivation of preexisting zones of weakness,
767 alkaline magmatism, and other tectonism postdating continental fragmentation,
768 *Reviews of Geophysics and Space Physics*, 4, 621-688.
769 https://doi.org/10.1029/RG016i004p00621

770 Tarayoun, A., Mazzotti, S., Craymer, M., & Henton, J. (2018). Structural inheritance control
771 on intraplate present-day deformation: GPS strain rate variations in the Saint
772 Lawrence Valley, eastern Canada, *Journal of Geophysical Research: Solid Earth*, in
773 press. https://doi.org/10.1029/2017JB015417

774 Thielmann, M., & Kaus, B. J. P. (2012). Shear heating induced lithospheric-scale localization:
775 Does it result in subduction?, *Earth and Planetary Science Letters*, 359-360, 1-13.
776 https://doi.org/10.1016/j.epsl.2012.10.002

777 Thomas, W. A. (2006). Tectonic inheritance at a continental margin. *GSA Today*, 16, 4-11.
778 https://doi.org/10.1130/1052-5173(2006)016[4:TIAACM]2.0.CO;2

779 Tommasi, A., Knoll, M., Vauchez, A., Signorelli, J. W., Thoraval, C., & Logé, R. (2009).
780 Structural reactivation in plate tectonics controlled by olivine crystal anisotropy,
781 *Nature Geoscience 2*, 423-429. https://doi.org/10.1038/ngeo528

782 Weertman, J. (1978). Creep laws for the mantle of the Earth, *Philosophical Transactions of*
783 *the Royal Society London*, A 288, 9-26

784 Wilks, K. R., & Carter, N. L. (1990). Rheology of some continental lower crustal rocks,
785 *Tectonophysics*, 182, 57-77. https://doi.org/10.1016/0040-1951(90)90342-6

786 Wintsch, R. P., Christoffersen, R., & Kronenberg, A. K. (1995). Fluid-rock reaction
787 weakening of fault zones, *Journal of Geophysical Research*, 100, 13021-13032.
788 https://doi.org/10.1029/94JB02622

789 Wu, P., & Johnston, P. (2000). Can deglication trigger earthquakes in N. America ?,
790 *Geophysical Research Letters*, 27, 1323-1326. https://doi.org/10.1029/1999GL011070

791 Wu, P., & Mazzotti, S. (2007). Effects of a lithospheric weak zone on postglacial
792 seismotectonics in eastern Canada and the northeastern United States. In S. Stein, & S.
793 Mazzotti, (Eds), Continental Intraplate Earthquakes: Science, Hazard, and Policy
794 Issues. *The Geological Society of America*, Special paper 425 (pp. 113-128).
795 https://doi.org/10.1130/2007.2425(09)

796 Zoback, M. D., & Townend, J. (2001). Implications of hydrostatic pore pressures and high
797 crustal strength for the deformation of intraplate lithosphere, *Tectonophysics*, 336, 19-
798 30. https://doi.org/10.1016/S0040-1951(01)00091-9